



# Silica-based photonic crystal fiber infiltrated with 1,2-dibromoethane for supercontinuum generation

HIEU LE VAN,<sup>1,\*</sup>  VAN THUY HOANG,<sup>2</sup> TRUNG LE CANH,<sup>2</sup> QUANG HO DINH,<sup>3</sup>   
HUE THI NGUYEN,<sup>1,4</sup> NGOC VO THI MINH,<sup>2</sup> MARIUSZ KLIMCZAK,<sup>4</sup>  RYSZARD BUCZYNSKI,<sup>4,5</sup>   
AND RAFAŁ KASZTELANIC<sup>4,5</sup> 

<sup>1</sup>Faculty of Natural Sciences, Hong Duc University, 565 Quang Trung Street, Thanh Hoa City, Vietnam

<sup>2</sup>Department of Physics, Vinh University, 182 Le Duan, Vinh City, Vietnam

<sup>3</sup>School of Chemistry, Biology and Environment, Vinh University, 182 Le Duan Street, Vinh City, Vietnam

<sup>4</sup>Faculty of Physics, University of Warsaw, Pasteura 5, 02-093 Warsaw, Poland

<sup>5</sup>Lukasiewicz Research Network - Institute of Microelectronic and Photonics, Aleja Lotników 32/46, 02-668 Warsaw, Poland

\*Corresponding author: [Levanhieu@hdu.edu.vn](mailto:Levanhieu@hdu.edu.vn)

Received 11 May 2021; revised 16 July 2021; accepted 20 July 2021; posted 20 July 2021 (Doc. ID 430843); published 16 August 2021

This study proposes a photonic crystal fiber (PCF) made of fused silica glass with the core infiltrated with 1,2-dibromoethane ( $C_2H_4Br_2$ ) as a new source of supercontinuum light pulses. Due to the modifications of the PCF's structure geometry, a number of computer simulations investigating their optimized structures has been carried out. This aimed at achieving flat near-zero dispersion and zero dispersion wavelength matching of the pump wavelength for efficient spectral broadening. Based on the obtained results, the structural geometries of two  $C_2H_4Br_2$ -core PCFs were optimized using numerical modeling for broadband supercontinuum (SC) generation. The first fiber structure with a lattice constant  $1.5\ \mu\text{m}$  and filling factor 0.4 has all-normal dispersion profile. The SC with a broadened spectral bandwidth from  $0.64$  to  $1.70\ \mu\text{m}$  is generated by pump pulses centered at a wavelength of  $1.03\ \mu\text{m}$ ,  $120\ \text{fs}$  duration, and energy of  $1.5\ \text{nJ}$ . The second proposed structure—with lattice constant  $1.5\ \mu\text{m}$  and filling factor 0.65—has anomalous dispersion for wavelengths longer than  $1.03\ \mu\text{m}$ . We obtained high coherence of the SC pulses in the anomalous dispersion range over wavelengths of  $0.7$ – $2.4\ \mu\text{m}$  with the same pump pulse as the first fiber and with input energy of  $0.09\ \text{nJ}$ . These fibers would be interesting candidates for all-fiber SC sources operating with low-energy pump lasers as cost-effective alternatives to glass core fibers. © 2021 Optical Society of America

<https://doi.org/10.1364/AO.430843>

## 1. INTRODUCTION

Fiber-based supercontinuum (SC) sources have been used widely in optical frequency metrology [1], ultrashort pulse generation [2], and telecommunication [3]. The approach required for coherent and spectrally broad SC generation is to use ultrashort laser pulses (subpicosecond durations) injected into nonlinear optical fibers in which the pulses are broadened via effects of dispersion and nonlinearity [4]. For the anomalous dispersion range of wavelengths, the soliton and soliton-related dynamics such as soliton fission, dispersive wave generation, and Raman soliton self-frequency shifting are significant contributors to the SC formation [5]. In such a case, SC has complex and nonuniform temporal profile, and unless specific conditions of input soliton order, pulse duration, and propagation length (among others) are met, it exhibits low coherence [6]. Meanwhile, in the case of all-normal dispersion (ANDi) operation, SC generation is induced by self-phase modulation (SPM)

and then followed by optical wave breaking (OWB) at the trailing and leading pulse edges [7]. The ANDi SC generation can preserve not only high coherence and a nearly tabletop flat spectrum but also pulse uniformity [8]. However, the ANDi SC usually requires much higher peak power of input laser pulses than SC generation pumped into anomalous dispersion wavelengths of the nonlinear medium [1].

Considerable effort has been devoted to extend the spectral width and to improve spectral flatness of SC sources. To achieve this, the PCF requires a special design for both flat all-normal dispersion and high-nonlinearity properties, and it should be optimized by means of the pump wavelength and input powers [9]. Various recent designs such as different core geometries [10] and multiple air-hole diameters in different rings [11] have been used to achieve ultra-flattened dispersion values over wider wavelength bandwidths. Those approaches have exploited the strong influence of geometrical properties of the first-ring air

hole on dispersion characteristics, particularly, zero dispersion wavelength (ZDW). However, the above-designed fiber structures are complicated and difficult for practical fabrication, so they are not commonly used.

Meanwhile, the high nonlinearity can be achieved by selection of glasses with higher nonlinearity than that of silica [12,13]. In reality, silica has exceptional purity and very high laser damage threshold, and hence silica-based optical fibers have been commonly used for SC generation. However, silica has low nonlinearity and limitation of the transmission band (below 2.5  $\mu\text{m}$ ) [14]. Otherwise, optical fibers made of soft glasses, such as tellurium chalcogenide [12] and chalcogenide [13], can offer the ANDi SC with spectral spanning up to 13.1  $\mu\text{m}$  [12]. These materials offer more broadband transmission windows into the mid-IR range than silica. Importantly, they provide high nonlinear refractive indices, so it is promising that the SC phenomena can take place on a significantly shorter propagation length [13] compared to low-nonlinearity fibers (such as silica fibers). However, these fibers are incompatible with silica for fusion splicing, have limited laser power handling capacity (low damage threshold), and also often require complex pumping systems because their dispersion profiles are very steep over a normal range of values at wavelengths where robust femtosecond lasers operate (i.e., 0.8–2.0  $\mu\text{m}$ ).

Recently, hollow-core fibers infiltrated with liquids have been proposed as an attractive approach for SC generation because the liquids have high nonlinearity and high transparency [15,16]. Work on SC generation with the use of liquid-infiltrated PCFs is currently on the rise [17–25]. The results obtained with liquid-filled-core PCFs during the recent years are briefly summarized in Table 1.

The obtained results indicated that the location of the ZDW can be adjusted and matched to the pump wavelength of high-power commercial lasers, and all-normal dispersion operation is also feasible [19–21]. As selected liquids have higher values of the nonlinear refractive index [13], we can obtain the broadband, coherent SC spectrum either in a few-centimeters-long liquid-core fiber sample or using lower peak power [15,20,22]. Additionally, it is also expected that using liquid-core PCFs allows control of the SC spectra by modification of temperature

or pressure, since it is possible to alter the dispersion properties of PCFs via these factors [26]. Some highly nonlinear liquids have wide transparency ranges in the mid-IR [16], which are beneficial for extending SC far into these wavelengths, where numerous application opportunities in different fields like medical diagnostics [24] or biomedical technologies [27] exist.

In this work, for the first time to our knowledge, we propose a  $\text{C}_2\text{H}_4\text{Br}_2$ -filled-core PCF for efficient and broadband near-IR SC generation. We have selected  $\text{C}_2\text{H}_4\text{Br}_2$  because it has a high nonlinear refractive index  $n_2 = 35 \times 10^{-20} \text{ m}^2/\text{W}$  at  $\lambda = 532 \text{ nm}$  [28]. Its nonlinearity is higher than that of fused silica ( $n_2 = 1.72 \times 10^{-20} \text{ m}^2/\text{W}$  [29]) and other liquids such as  $\text{CCl}_4$  ( $n_2 = 1.53 \times 10^{-19} \text{ m}^2/\text{W}$ ) [20],  $\text{CHCl}_3$  ( $n_2 = 1.64 \times 10^{-19} \text{ m}^2/\text{W}$ ) [22], and  $\text{C}_2\text{Cl}_4$  ( $n_2 = 1.675 \times 10^{-19} \text{ m}^2/\text{W}$ ) [19]. In addition,  $\text{C}_2\text{H}_4\text{Br}_2$  is transparent from the visible to the near-IR. We show that, by filling the core with  $\text{C}_2\text{H}_4\text{Br}_2$ , we can adjust the dispersion characteristic of the PCF, achieving flat and low dispersion with the wavelength of maximum dispersion close to the pump wavelength. For those optimum fiber structures, we utilized the generalized nonlinear Schrödinger equation (GNLSE) to demonstrate SC generation numerically. The coherence of SC generation with the effects of vacuum noise and pulse-to-pulse relative intensity noise is also numerically investigated.

The paper is organized as follows. In Section 2, we describe the proposed microstructured PCF with a liquid-filled core. Section 3 shows how the fiber can be optimized to obtain flat and low dispersion characteristics numerically. The SC spectra generated in the optimized PCFs are also described in this section. The paper ends with the conclusion in Section 4.

## 2. PROPOSED MICROSTRUCTURED PHOTONIC CRYSTAL FIBER

### A. Fiber Structure

In this section, we consider PCFs made of fused-silica glass, which have the core filled with  $\text{C}_2\text{H}_4\text{Br}_2$ . The geometry of the designed PCF is schematically shown in Fig. 1. The fiber consists of eight air-hole rings arranged in a regular lattice defined

**Table 1. Overview SC Generation in Several Liquid-Core PCFs**

Liquid-Core PCFs	Year	Pump Wavelength ( $\mu\text{m}$ )	Regime	SC Range (nm)	Refs.
$\text{CS}_2$	2006	1.55	Normal	700–2500	[17]
	2016	1.55	Normal	1355–2110	[18]
$\text{C}_7\text{H}_8$	2017	1.55	Normal	1100–1750	[19]
			Anomalous	1000–1750	
$\text{CCl}_4$	2018	1.35	Anomalous	800–2200	[20]
			Normal	1000–2100	
	2019	1.03	Normal	850–1250	[21]
$\text{CHCl}_3$	2019	1.03	Normal	600–1260	[22]
			Anomalous	600–1400	
$\text{C}_6\text{H}_5\text{NO}_2$	2020	1.03	Normal	700–1700	[23]
			Normal	800–2100	
			Anomalous	1300–2300	
$\text{C}_2\text{Cl}_4$	2018	1.92	Anomalous	1100–2400	[24]
			Normal	700–2400	[25]
	2021	1.56	Normal	800–2000	
			Anomalous	1000–2000	

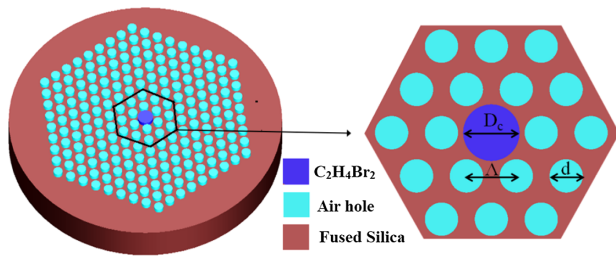


**Fig. 1.** Schematic of the modeled PCF structure;  $D_c$  is the diameter of the liquid-filled core.

by the lattice pitch  $\Lambda$  and air-hole diameter  $d$ . The filling factor of the fiber is defined as  $f = d/\Lambda$ . The diameter of the core is determined by the formula  $D_c = 2\Lambda - 1.2d$  to ensure technical feasibilities of the proposed structures after fabrication procedures.

We used commercial software Lumerical MODE solutions with the full-vector finite-difference eigenmode (FDE) method to achieve the field intensity profile of the fundamental mode of the PCFs [30]. Here, the boundary condition for simulation is a perfectly matched layer, which allows enhancement of the numerical accuracy of simulations and reduces the meshing errors.

### B. Linear Parameters of the Selected Liquid

Group refractive index  $N$  of  $C_2H_4Br_2$  was measured using the white-light interferometric technique. The material dispersion of the liquid was measured using a standard Michelson interferometer. Its setup is schematically shown in Fig. 2.

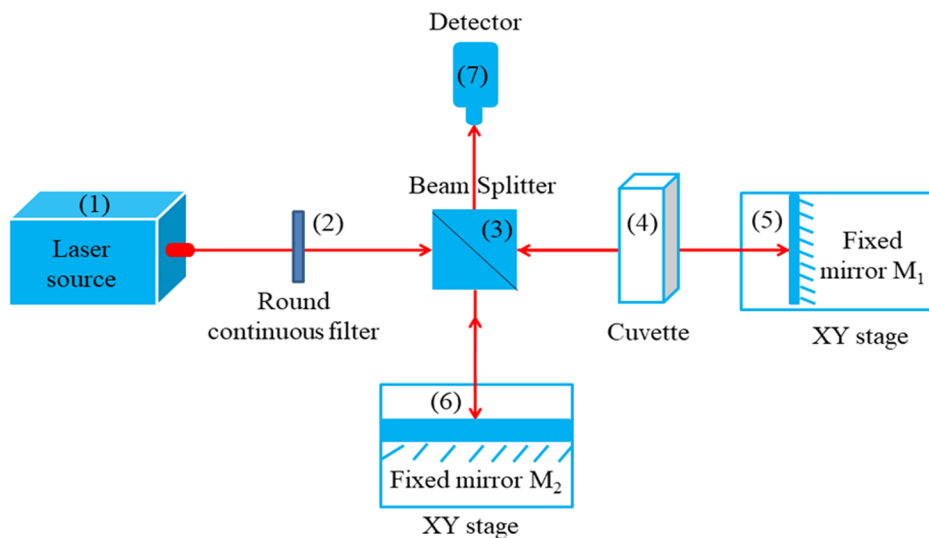


**Fig. 2.** Scheme of the setup for material dispersion of  $C_2H_4Br_2$ : (1) SuperK Compact Laser Source; (2) round continuous filter; (3) beam splitter; (4) fixed mirror  $M_1$ ; (5) cuvette; (6) fixed mirror  $M_2$ ; and (7) detector.

In this setup, the incident beam is split by a 50:50 beam splitter (BS13, Thorlabs) into two equal parts. One of them passes through a cuvette containing a liquid sample (main arm), and the other one plays the role of a reference beam (reference arm) for the interferometer configuration. In the reference arm, a mirror  $M_1$  is attached to a high-precision translation stage (Nanomax 350D/M, Thorlabs) for manipulation during measurements. This allows compensation and measurement of optical path difference (OPD) caused by the liquid sample in the main arm. The interference patterns are recorded by suitable detectors connected with spectrometers operating in the visible and near-IR spectral range (Red Tide, Ocean Optics, and AvaSpec-NIR256/512-1.7). The OPD is calculated as a function of wavelength, which allows determination of how the obtained spectral range depends on group refractive index  $N$  [31]. The resulted curve is fitted by the function  $N(\lambda)$  described in Eq. (1). Here, the phase refractive index  $n(\lambda)$  is given by the Sellmeier formula as in Eq. (2). Values of the used Sellmeier coefficients for the fused silica and  $C_2H_4Br_2$  are presented in Table 2. Parameters  $n$ ,  $\lambda$  are the refractive index of the liquid and the wavelength, respectively.

$$N(\lambda) = n(\lambda) + \frac{\lambda^2}{n(\lambda)} \sum_{i=1}^3 \frac{B_i C_i}{(\lambda^2 - C_i^2)}, \quad (1)$$

$$n = \sqrt{1 + \frac{B_1 \lambda^2}{\lambda^2 - C_1} + \frac{B_2 \lambda^2}{\lambda^2 - C_2} + \frac{B_3 \lambda^2}{\lambda^2 - C_3}}. \quad (2)$$

The group and phase refractive indices of  $C_2H_4Br_2$  were calculated and depicted in Fig. 3. The obtained results are similar to

**Table 2.** Sellmeier Coefficients of the Materials Used

Materials	Sellmeier Coefficients					
	$B_1$	$C_1$ [ $\mu\text{m}^2$ ]	$B_2$	$C_2$ [ $\mu\text{m}^2$ ]	$B_3$	$C_3$ [ $\mu\text{m}^2$ ]
Fused silica [19]	0.6694226	$4.4801 \times 10^{-3}$	0.434584	$1.3285 \times 10^{-2}$	0.8716947	95.341482
$C_2H_4Br_2$	1.3163728	0.01616122	0.4013224	142.2298902	-	-

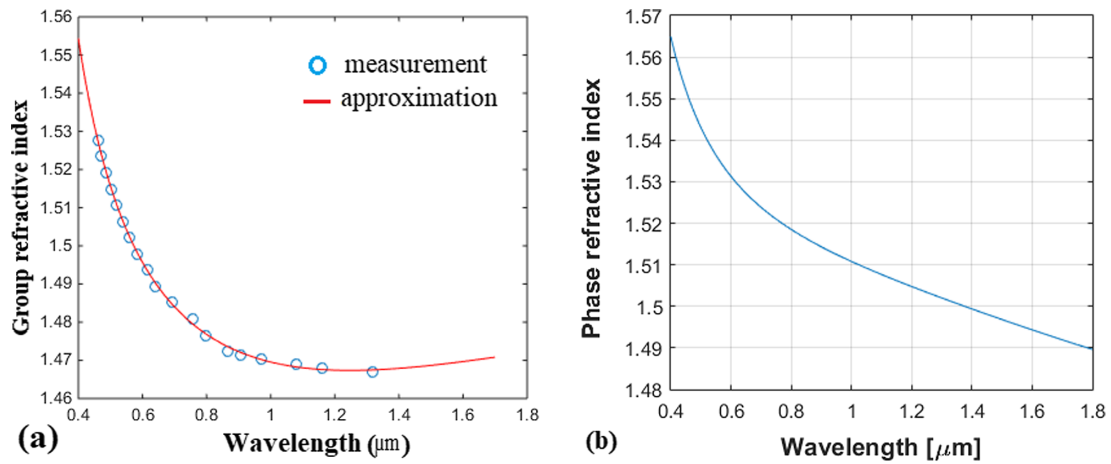


Fig. 3. (a) Group and (b) phase refractive indices measured for the investigated liquid.

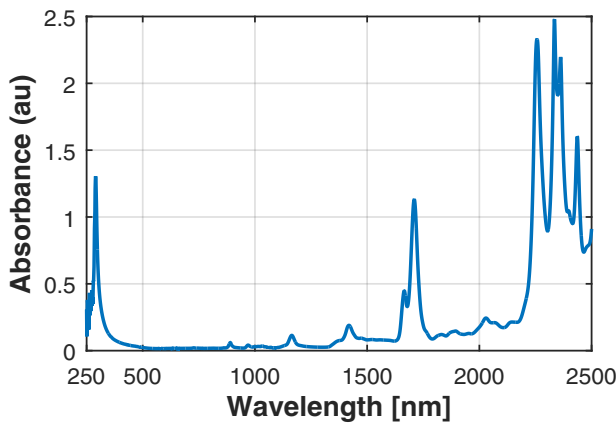


Fig. 4. Absorbance spectra for  $C_2H_4Br_2$  for a standard high-quality fused silica cuvette with a square cross section ( $10 \times 10$  mm and 100  $\mu$ m thick walls).

the that previously reported in [32], which confirmed the accuracy of our experimental results.

The absorbance characteristic of the  $C_2H_4Br_2$  in the spectral range of 250–2500 nm is shown in Fig. 4. The absorbance measurement was performed by using spectrophotometers operating in the visible and near-infrared spectral range (Agilent 8453 optics and DW-S430). The liquid has four main absorption peaks at 300, 1700, 2300, and 2400 nm. Meanwhile, it has minimum absorption around the wavelength of 1030 nm and high transparency in the range from 350 to 1650 nm.

### C. Modeling of SC Generation

The propagation of an optical pulse whose field amplitude changes slowly can be described by the GNLSE [5]:

$$\frac{\partial A}{\partial z} + \frac{\alpha}{2}A + \sum_{n=2}^{\infty} i^{(n-1)} \frac{\beta_n \partial^n A}{n! \partial t^n} = i\gamma \left( 1 + \frac{i}{\omega_0} \frac{\partial}{\partial t} \right) A(z, t) \left[ \int_{-\infty}^{\infty} R(t') |A(z, t-t')|^2 dt' \right], \tag{3}$$

where  $z$ ,  $\alpha$ , and  $\beta_n$  are the spatial coordinate along the fiber, the total loss, and the  $n$ th order of dispersion of the PCF, respectively.

The terms on the right-hand side of Eq. (3) represent nonlinearity in the optical fiber and include contributions from the Kerr effect and Raman effect. Meanwhile, the nonlinear parameter  $\gamma$  of the fiber is defined as [5]

$$\gamma(\lambda) = \frac{2\pi n_2}{\lambda A_{\text{eff}}}, \tag{4}$$

where  $A_{\text{eff}}$  is the effective mode area of the fiber and  $n_2$  is the nonlinear refractive index of  $C_2H_4Br_2$ .

The effective mode area  $A_{\text{eff}}$  is computed from [5]

$$A_{\text{eff}} = \frac{(\iint |E|^2 dx dy)^2}{\iint |E|^4 dx dy}, \tag{5}$$

where  $E(x, y)$  is the field distribution of the fiber mode.

The other nonlinear term in Eq. (3) represents the Raman response. It should contain the main contributions as the electronic and vibrational parts. Taking the assumption that the electronic factor is contributed instantaneously, the Raman response function  $R_r$  can be written as [5]

$$R(t) = (1 - f_R)\delta(t) + f_R h_R(t), \tag{6}$$

where  $\delta(t)$  is the Dirac delta function and  $f_R$  represents the fractional contribution of the delayed Raman response function  $h_R(t)$ , which in turn takes an approximate analytical form [5]:

$$h_R(t) = \frac{\tau_1^2 + \tau_2^2}{\tau_1 \tau_2} \exp(-t/\tau_2) \sin(-t/\tau_1), \tag{7}$$

where  $\tau_1 = 4.246$  fs and  $\tau_2 = 30.33$  fs for  $C_2H_4Br_2$  [33,34].

The coherence properties of the SC pulses obtained from the designed PCFs are investigated theoretically by including the one-photon-per-mode noise. The relation for the coherence degree is then as follows [35]:

$$\left| g_{12}^{(1)}(\lambda, t_1 - t_2 = 0) \right| = \left| \frac{E_1^*(\lambda, t_1) E_2(\lambda, t_2)}{[|E_1(\lambda, t_1)|^2 |E_2(\lambda, t_2)|^2]^{1/2}} \right|, \tag{8}$$

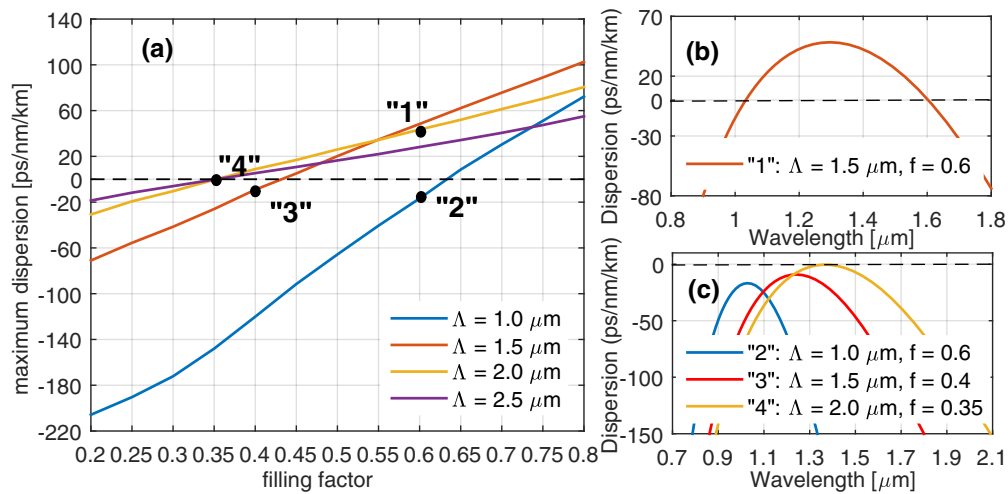


**Fig. 5.** Numerical simulation of the dispersion characteristics in the fundamental mode of the PCFs: (a) the maximum dispersion for various lattice pitch  $\Lambda$  and filling factors  $f$ ; (b) PCF with both normal and anomalous dispersion; (c) PCF with all-normal dispersion.

where  $E_1(\lambda)$  and  $E_2(\lambda)$  are the amplitudes of the electric field for two successive generated spectra. The value of  $g_{12}^{(1)}$  is in the range of  $[0, 1]$ , where  $g_{12}^{(1)} = 1$  for a high coherent spectrum, and  $g_{12}^{(1)} = 0$  for incoherent light.

The coherence of the generated SC pulses depends on the effects of the input noise, such as vacuum noise, pulse-to-pulse relative intensity noise (RIN), and polarization noise [36]. However, in the case of short pump pulse duration, previous theoretical studies have speculated that polarization noise could be neglected [37], and hence in here we estimate the coherence in SC generation with the influence of vacuum noise (shot noise) and the pulse-to-pulse relative intensity noise.

### 3. NUMERICAL RESULTS

#### A. Fiber Dispersion Engineering

Our purpose is to design and simulate fibers for SC generation at the selected pump wavelength of  $1.03 \mu\text{m}$  with high coherence and flat spectrum in the wide range of wavelengths from the visible to the near-IR. With this aim, we initially considered the PCFs with  $\Lambda$  changing from  $1.0$  to  $2.5 \mu\text{m}$  with steps of  $0.5 \mu\text{m}$  and  $f$  changing from  $0.2$  to  $0.8$  with steps of  $0.05$ . A set of simulations has been performed to study the flat, low dispersion characteristics and the difference between ZDW and pump wavelength. All these numerical calculations were carried out for the wavelength range of  $0.5$ – $2.0 \mu\text{m}$ .

The maximum dispersion of the fundamental mode is illustrated in Fig. 5(a) for different lattice pitch  $\Lambda$  and filling factor  $f$ . In all cases, the dispersion profile takes normal values, except for some structures, where the local maximum appears in the anomalous dispersion range (and there are two ZDWs). Figure 5(c) shows an example the dispersion characteristic of the PCF in the all-normal dispersion regime at locations 2, 3, and 4 in Fig. 5(a). In this manner, the maximum dispersion increases with increasing  $f$  for a constant  $\Lambda$ . Similar behavior is also observed when the filling factor is constant but increases the lattice pitches. Moreover, increasing the lattice pitch can make the dispersion flatter, and it eventually becomes monotonic.

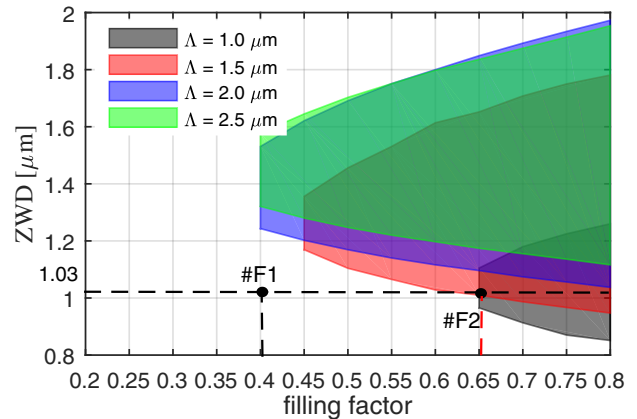


**Fig. 6.** Shifts of ZDWs with changing lattice pitch  $\Lambda$  and filling factors  $f$ . Two fibers #F1 and #F2, considered in detail later, are highlighted.

Figure 6 illustrates the ZDW shift with different  $\Lambda$  and  $f$ . For a certain value of  $\Lambda$ , increasing the filling factor leads to ZDW shifting toward the shorter wavelengths. In the opposite case, for a certain value of  $f$ , the ZDW will be shifted toward longer wavelengths if  $\Lambda$  is increased. Specifically, there are two ZDWs appearing in several areas such as the dark area (corresponding with  $\Lambda = 1.0 \mu\text{m}$  and  $f$  changing from  $0.65$  to  $0.8$ ), red area (corresponding with  $\Lambda = 1.5 \mu\text{m}$  and  $f$  changing from  $0.45$  to  $0.8$ ), blue area, and green area (corresponding with  $\Lambda = 2.0 \mu\text{m}$  and  $\Lambda = 2.5 \mu\text{m}$ ,  $f$  changing from  $0.4$  to  $0.8$ , respectively). In the rest of the cases, for the left of the dark area, corresponding to the fibers with  $\Lambda = 1.0 \mu\text{m}$ , it is fulfilled for  $f$  from  $0.2$  to  $0.6$ . It is fulfilled from  $0.2$  to  $0.45$  for fibers with  $\Lambda = 1.5 \mu\text{m}$  to the left of the red area (decreasing filling factors), and from  $0.2$  to  $0.4$  for fibers with  $\Lambda = 2.0 \mu\text{m}$  to the left of the blue area. For a fiber with  $\Lambda = 2.5 \mu\text{m}$  left of the green area, the proposed fiber structure with all-normal dispersion has no ZDW.

Basing on these preliminary calculations, we proposed two PCFs, namely, #F1 and #F2. Their geometrical parameters are listed in Table 3.

**Table 3. Geometrical Parameters for Selected Structures**

Parameter	#F <sub>1</sub>	#F <sub>2</sub>
Lattice pitch $\Lambda$ [ $\mu\text{m}$ ]	1.5	1.5
Filling factor $f = d / \Lambda$	0.4	0.65
Cladding holes diameter $d$ [ $\mu\text{m}$ ]	0.6	0.975
Core diameter $D_c$ [ $\mu\text{m}$ ]	2.28	1.83

The first fiber (#F<sub>1</sub>) is modeled to work in the normal dispersion range under pumping centered at a wavelength of 1.03  $\mu\text{m}$ . This PCF type has no ZDW as discussed in the previous section (Fig. 6). Although fibers having  $\Lambda = 1.0 \mu\text{m}$  [an in example as 2 in Fig. 5(a)] have ANDi with  $f$  values less than 0.6, their dispersion curves show less flatness than ones with  $\Lambda = 1.5 \mu\text{m}$ . Moreover, in the former case, the wavelength located at the dispersion maximum is much lower from the horizontal axis. In principle, we can obtain the largest bandwidth of the generated SC spectrum by using the pump wavelength being near the one at the local maximum point of a dispersion curve. Here, when  $f$  changes from 0.2 to 0.4, fibers with  $\Lambda = 2.0 \mu\text{m}$  or  $\Lambda = 2.5 \mu\text{m}$  can also perform ANDi with properties especially favorable for efficient SC generation, i.e., low and flatter dispersion, although the wavelength located at the maximum point of the dispersion curve is farther from the pump wavelength than in the case of fibers with  $\Lambda = 1.5 \mu\text{m}$  [see Fig. 5(c)]. Therefore, the fiber with  $\Lambda = 1.5 \mu\text{m}$ ,  $f = 0.4$  was selected as the optimum (point #F<sub>1</sub> in Fig. 6).

For the second fiber #F<sub>2</sub> with  $\Lambda = 1.5 \mu\text{m}$ ,  $f = 0.65$  (point #F<sub>2</sub> in Fig. 6), which is expected to produce the highly coherent SC pulses in the regime of anomalous dispersion with pump wavelength of 1.03  $\mu\text{m}$ . This fiber was selected because it has the first ZDW at 1.01  $\mu\text{m}$ , which is the closest to the wavelength used for pumping. Another reason is that the calculated dispersion at 1.03  $\mu\text{m}$  equals 18.5 ps/nm/km, which is also the closest value to the zero dispersion for all dispersion characteristics computed for structures with  $\Lambda = 1.5 \mu\text{m}$ .

Figure 7 shows the computer calculated chromatic dispersion curves of the fundamental propagation mode in two proposed fibers by the use of a commercial software MODE solution with the full-vector finite-difference method [30].

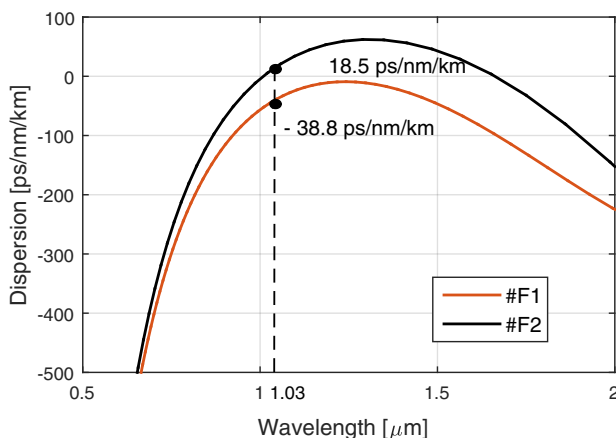


**Fig. 7.** Dispersion characteristics of the fundamental mode for fibers #F<sub>1</sub> and #F<sub>2</sub>.

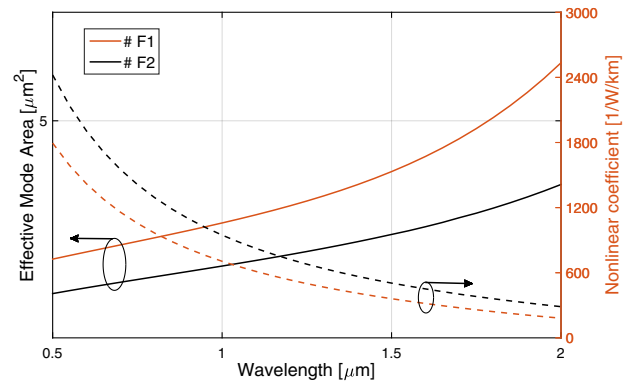


**Fig. 8.** The effective mode areas and nonlinear coefficients of the proposed PCFs. The solid lines and dashed lines denotes for mode area and nonlinear coefficient, respectively.

Fiber #F<sub>1</sub> exhibits all-normal dispersion in the whole analyzed wavelength range, and the dispersion at 1.03  $\mu\text{m}$  equals  $-38.8 \text{ ps/nm/km}$ , while fiber #F<sub>2</sub> has the first ZDW at 1.01  $\mu\text{m}$  and the value of dispersion calculated at the pump wavelength is  $18.5 \text{ ps/nm/km}$ .

The nonlinear coefficients and effective mode areas of the proposed fiber structures are shown in Fig. 8. In particular, the nonlinear coefficient  $\gamma$  of fibers can be obtained by Eq. (4). The obtained results indicate that the mode area of the fundamental mode increases with the wavelength in both cases. The mode effective area for the fundamental modes of fibers #F<sub>1</sub> and #F<sub>2</sub> are  $3.132 \mu\text{m}^2$ , and  $2.18525 \mu\text{m}^2$  for a pump wavelength of 1.03  $\mu\text{m}$ , while their nonlinear coefficients are  $681.35 \text{ W}^{-1} \cdot \text{km}^{-1}$  and  $976.538 \text{ W}^{-1} \cdot \text{km}^{-1}$ , respectively.

### B. Supercontinuum Generation in Proposed PCFs

The SC generation in the proposed fibers was investigated using input pulses with a pump wavelength at 1.03  $\mu\text{m}$ , pulse duration of 120 fs, and various input powers, which is available from different robust femtosecond ytterbium fiber laser devices (e.g., Menlo Systems, Germany, or Toptica, Germany, or IMRA, USA).

Figure 9(a) shows the simulated SC spectra for various input powers in 10 cm propagation length for fiber #F<sub>1</sub>. As shown by the obtained results, the spectral width will increase with an increase in input power. In the case of input power of 12.5 kW, the spectral bandwidth extends from 0.64 to 1.70  $\mu\text{m}$  within a 10 dB dynamic range [Fig. 9(a)]. Meanwhile, Fig. 9(b) depicts the evolution of SC and the temporal profile at different positions of propagation lengths. At the beginning of the fiber, the spectrum of the pulses expands due to the strong self-phase modulation (SPM) effect when pumping in the normal dispersion regime. The obtained spectrum is asymmetric toward the shorter wavelengths due to combined linear (dispersion) and nonlinear (self-steeping) effects. The SPM-induced spectrum experiences effects of the dispersion in further propagation, and the short wavelengths at the trailing edge propagate more slowly than the pulse at the center of the pulse. The overlap between the pulse tail and trailing edge would generate the new wavelengths by four-wave mixing (FWM), which are attributed to optical wave breaking.

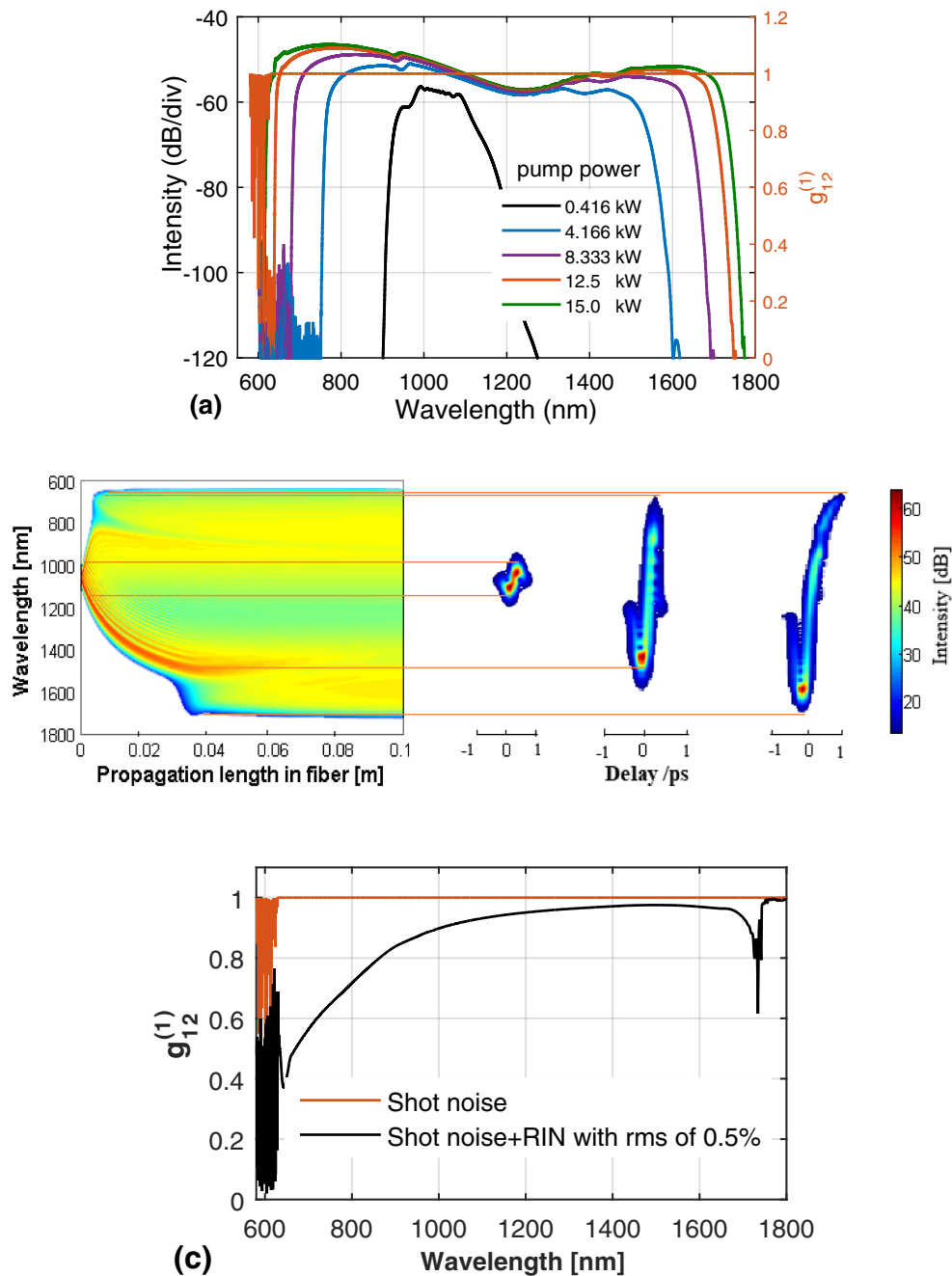


**Fig. 9.** Numerical calculations of the SC generation: (a) the output spectrum for various input powers in 10 cm propagation length when pump pulse with  $1.03 \mu\text{m}$  pump wavelength, 120 fs duration, and the first-order coherence is calculated with 20 dB bandwidth with random single-photon-per-mode noise seeds for 1.5 nJ energy, corresponding to  $P_0 = 12.5 \text{ kW}$ ; (b) temporal evolutions of SC spectrum and temporal profile at different propagation length, (c) effects of shot noise and RIN with rms of 0.5% in coherence of SC generation for  $\#F_1$ .

As depicted in Fig. 9(b), OWB begins creating a new wavelength around 750 nm at the pulse trailing edge of 1.0 cm propagation length. On the leading edge, OWB occurs only after 3.5 cm of propagation and creates a new band of wavelengths around 1700 nm. After a propagation length of 4.0 cm, the spectrum is no longer broadened due to the steep integrated dispersion curve on both sides.

The first-order degree of coherence is calculated with 20 dB bandwidth with random single-photon-per-mode

noise seeds. It is shown that highly coherent of the SC spectrum can be obtained due to its value is approximately 1 over the spectrum as shown in Fig. 9(a). Figure 9(c) presents the coherence of SC with effects of shot noise and RIN, where RIN is derived from the intensity fluctuation of input pulses with root mean square (rms) of 0.5%. The coherence is further decreased if the RIN is taken into account. Its value is approximately 1 for the case of shot noise, while in the case of RIN with rms of 0.5% has  $g_{12}^{(1)} < 0.97$ , and this

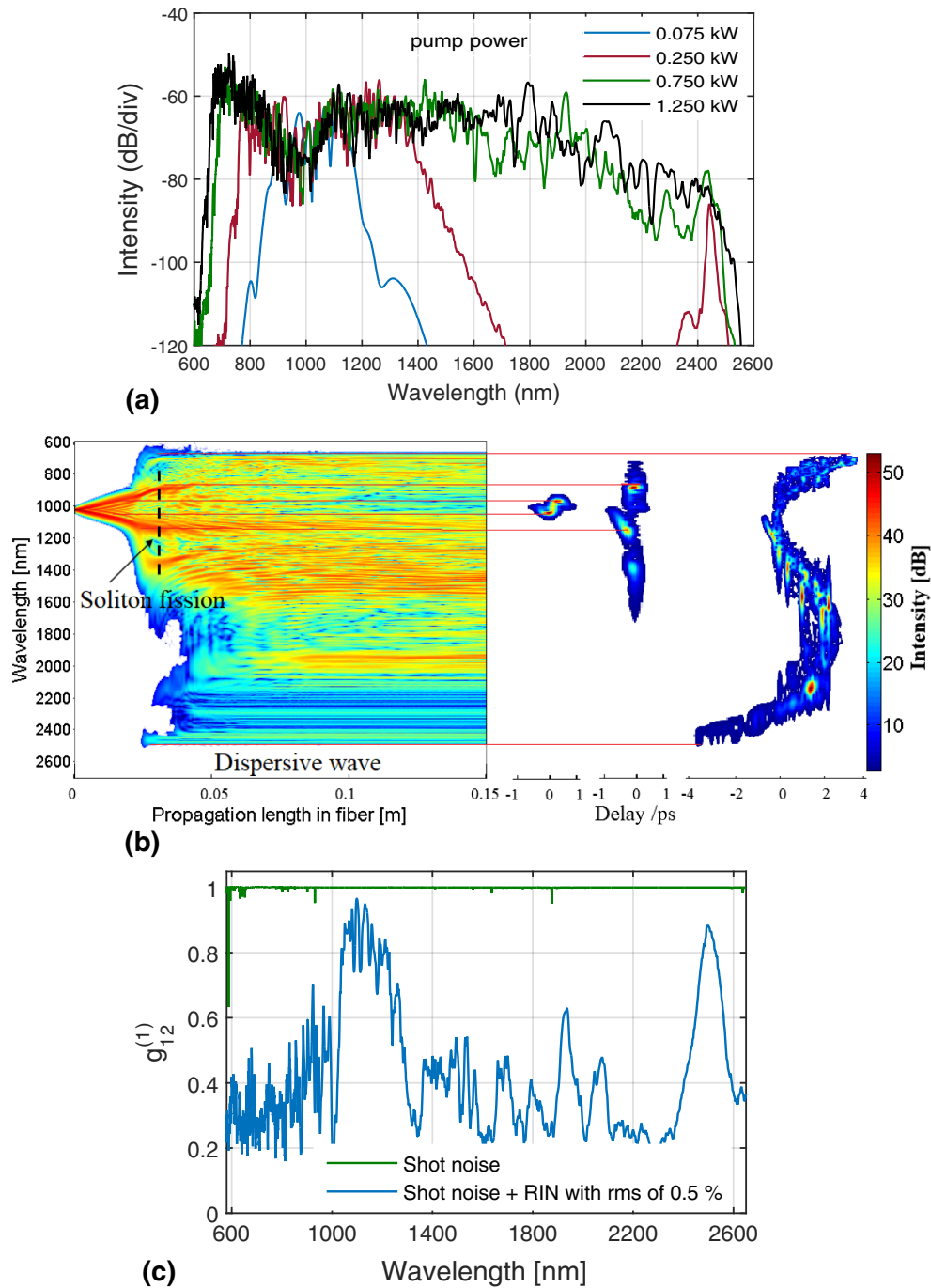


**Fig. 10.** Numerical calculations of the SC generation: (a) the output spectrum traces averaged over 10 shots performed under various input powers at 15 cm propagation length when using pump pulses with 1.03  $\mu\text{m}$  pump wavelength and 120 fs duration; (b) evolution of the SC spectrum along fiber and temporal profile at different propagation lengths; (c) effects of shot noise and RIN with rms of 0.5% in coherent SC generation for 0.09 nJ energy, corresponding to  $P_0 = 0.75 \text{ kW}$  for #F<sub>2</sub>.

value decreases very rapidly for wavelengths shorter than 1000 nm.

In the next case, fiber #F<sub>2</sub> provides two ZDWs at 1.01  $\mu\text{m}$  ( $\lambda_{\text{ZWD1}}$ ) and 1.66  $\mu\text{m}$  ( $\lambda_{\text{ZWD2}}$ ); the pump wavelength of 1.03  $\mu\text{m}$  is located in the regime of anomalous dispersion and near the ZDW  $\lambda_{D1}$ . Here, soliton dynamics, e.g., self-frequency shifting and soliton fission [4], would play an essential role in the broad of SC spectrum. During further propagation,

the solitons would shift toward the longer wavelengths due to soliton self-frequency shifts, causing a considerable spectral expansion toward the redshifted wavelengths. Upon crossing of the ZDWs, dispersive waves mainly contribute to the generation of new wavelengths.

Figure 10(a) shows obtained SC spectrum traces averaged over 10 shots performed under different powers at 15 cm of propagation length. With increasing pump powers, it can be

seen that the SC spectrum broadens dynamically. The spectral broadening comes, however, at the expense of very complex temporal pulse structuring with quite high noise. However, the amplification of noise caused by modulation instability can be reduced if using the pump wavelength in the normal dispersion and near-zero anomalous dispersion regimes or by reducing the pulse duration.

The characteristic lengths of pulse-broadening dynamics in #F<sub>2</sub> fiber are calculated using the following equation:

$$L_D = \frac{t_0^2}{|\beta_2|}, L_{NL} = \frac{1}{\gamma P_0}, L_{MI} = 16L_{NL}, N = \sqrt{\frac{L_D}{L_{NL}}}, L_{fiss} = \frac{L_D}{N}, \quad (9)$$

where  $L_D$ ,  $L_{NL}$ ,  $L_{MI}$ , and  $L_{fiss}$  are the dispersive, nonlinear, modulation instability, and soliton fission characteristic length scales, respectively.  $P_0$  is the peak power, and  $t_0$  is the pulse duration of the input pulse. The parameter  $\beta_2$  represents the group velocity dispersion coefficient.  $N$  is the soliton number.

For the case of input power  $P_0 = 0.75$  kW with corresponding pulse energy of 0.09 nJ, the dispersion length  $L_D$  is 143 cm, the nonlinear length  $L_{NL}$  is 0.14 cm, and the modulation instability length  $L_{MI}$  is 2.24 cm. Thus, the soliton number  $N$  is 32,

and the soliton fission length  $L_{fiss}$  is 4.4 cm, which matches well with data in Fig. 10(b). The spectral band extends from 700 to 2400 nm within a 30 dB dynamic range as shown in Fig. 10(a). The SC evolution and the temporal profile at different propagation lengths are depicted in Fig. 10(b). It is obvious that the main contributor to the spectral broadening of the propagation is SPM. Since pump wavelength (1.03  $\mu\text{m}$ ) is close to the ZDW (1.01  $\mu\text{m}$ ), a fraction of the spectrum is induced by SPM across the ZDW and experienced in the normal dispersion regime before soliton fission occurs. The soliton fission appears at 4.4 cm of propagation length, and then it is supported by FWM. After soliton fission, the spectrum would be influenced by the dispersive wave at the trailing edge as presented in Fig. 10(b).

The coherence of SC generation in #F<sub>2</sub> fiber is shown in Fig. 10(c). Its value is approximately 1 for the case including the shot noise. This means that coherent SC pulses can also be obtained in physical conditions (which involve laser shot noise). In the case of RIN with rms of 0.5 %, the pulse-to-pulse relative intensity noise causes fluctuation of the fundamental solitons, leading to the intensity and phase fluctuation of the related dispersive waves as well. Thus, the coherence is significantly decreased (average of the coherence  $\langle |g_{12}^{(1)}| \rangle = 0.4978$ ).

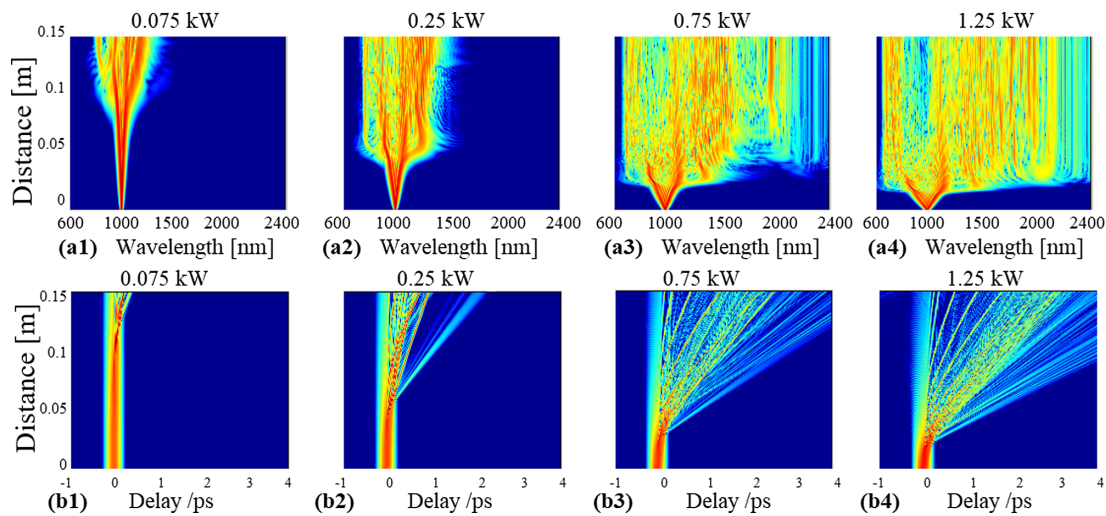


**Fig. 11.** (a1)–(a5) Evolution of the SC along fiber and (b1)–(b5) corresponding temporal profile with various input powers in 15 cm length when using pump pulse with 1.03  $\mu\text{m}$  pump wavelength and 120 fs duration for #F<sub>2</sub>.

**Table 4.** Summary of Properties for the Two Proposed PCFs #F<sub>1</sub> and #F<sub>2</sub>

Parameter	#F <sub>1</sub>	#F <sub>2</sub>
Fiber length [cm]	10	15
Coupled peak power [kW]	12.5	0.75
Bandwidth [THz]	176.348–468.426	124.913–428.275
Spectral range [nm]	640–1700	700–2400
$g_{12}^{(1)}$	Shot noise	high coherence
	Shot noise + RIN (0.5%)	moderate coherence
$L_D$	75.79	143
$L_{NL}$	0.12	0.14
$L_{MI}$	1.92	2.24
$L_{fiss}$	—	4.4
Main physical processes	SPM, MI, OWB, FWM	SPM, soliton fission, dispersive waves

Figures 11(a1)–11(a4) depict the resulting spectrum evolving along the proposed fiber with various peak pump powers. The corresponding temporal evolutions are presented in Figs. 11(b1)–11(b4). In each case, because different frequency components usually have different group velocities, the time delay between different frequencies becomes larger with longer propagation. Meanwhile, higher pump pulse energy also causes the time delay between difference frequencies occurring sooner with shorter distance as presented in Figs. 11(b1)–11(b4).

The comparison between the properties of the two proposed PCFs is presented in Table 4. As can be seen, the generated SC is almost perfectly coherent in the case of fiber #F<sub>1</sub> when the fiber is pumped at normal dispersion wavelengths. This is not surprising, since modulation instability and soliton-related effects are either suppressed or inhibited (respectively) in this case. This is thus a proposed structure to ensure coherent SC generation. However, the drawback is that the SC spectral width is comparatively much smaller than obtained from fiber #F<sub>2</sub>.

#### 4. CONCLUSION

In this work, we proposed PCFs made of fused silica with a C<sub>2</sub>H<sub>4</sub>Br<sub>2</sub>-filled core to obtain both all-normal dispersion or anomalous dispersion characteristics. We used a Michelson interferometer to measure the refractive index of the selected liquid. Moreover, we also measured the absorbance characteristic of C<sub>2</sub>H<sub>4</sub>Br<sub>2</sub> in the wavelength range of 250–2500 nm. With the modifications of structure geometry, a number of computer simulations looking for optimized PCF structures have been conducted. This aimed at achieving flat near-zero dispersion, low absolute dispersion, and ZDW matching with the pump center wavelength in order to facilitate the generation of spectrally broad SC pulses. As a result, optimized fiber #F<sub>1</sub> with lattice constant  $\Lambda = 1.5 \mu\text{m}$  and filling factor  $f = 0.4$  had the all-normal dispersion, and its peak equals  $-38.8 \text{ ps/nm/km}$  at  $1.03 \mu\text{m}$ . Fiber #F<sub>2</sub> with  $\Lambda = 1.5 \mu\text{m}$ ,  $f = 0.65$  has two ZDWs at  $1.01 \mu\text{m}$  and  $1.66 \mu\text{m}$ . For this fiber, the dispersion at  $1.03 \mu\text{m}$  is  $18.5 \text{ ps/nm/km}$ .

The PCF with the aforementioned parameters allows highly efficient coupling with standard femtosecond fibers and high fiber nonlinearity. It is well known that, using moderate input pulse peak powers of 10 kW with 120 fs pulse duration, it is possible to obtain SC with low-cost commercial femtosecond fiber lasers emitting at  $1.03 \mu\text{m}$ . Here we showed that coherent, octave-spanning SC pulses in fiber #F<sub>1</sub> could be obtained in the wavelength range of  $0.64$  to  $1.70 \mu\text{m}$  when using a pulse source with central pump wavelength of  $1.03 \mu\text{m}$ , 120 fs duration, and 1.5 nJ energy, corresponding to  $P_0 = 12.5 \text{ kW}$  input peak power. Meanwhile, fiber #F<sub>2</sub> produced a highly coherent SC with pumped wavelength at anomalous dispersion regime pumping. In this case, the SC was dominated by soliton dynamics, in which the solitons are propagated at wavelengths with anomalous dispersion, and in the normal dispersion wavelengths the spectral broadening is induced by the dispersive waves. With the same pump conditions as those used with fiber #F<sub>1</sub> and with input energy of 0.09 nJ, the corresponding input power of 0.75 kW, fiber #F<sub>2</sub> can enable highly coherent SC pulse generation pumped in the an anomalous dispersion range with spectral coverage from  $0.7$  to  $2.4 \mu\text{m}$ .

The advantage of using C<sub>2</sub>H<sub>4</sub>Br<sub>2</sub> as the nonlinear medium infiltrating a hollow-fiber core is that its nonlinear refractive index is higher than that of fused silica or some other liquids. Thus, lower power of input pulses is required to achieve the comparable SC bandwidth [17,18]. Owing to high nonlinearity and femtosecond-scale pump pulse duration, octave-spanning SC can be obtained in a short length of the fiber (10 cm). The use of short input pulse, combined with short fiber lengths, allowed suppression of the effects of polarization noise, Raman noise, and laser noise, which normally manifest in coherence degradation [38,39]. The practical dimension and advantage of the proposed fibers would be the decrease of the peak power requirement, which would make the necessary femtosecond pump source a relatively robust fiber-based laser, instead of a complex optical parametric chirped-pulse amplifier. In fact, the coherent and octave-spanning SC with low input pulse power can be applied for, e.g., on-chip frequency metrology [40]. Importantly, our research shows the compatibility of these designed PCF structures, with standard, fixed-wavelength femtosecond lasers operating at  $1.03 \mu\text{m}$ , which could be used as optical pump sources for SC generation. The low pump pulse requirement presents an interesting perspective of the C<sub>2</sub>H<sub>4</sub>Br<sub>2</sub>-filled PCFs in the easing of the output power requirements on the femtosecond mode-locked lasers, which is necessary to obtain octave-spanning bandwidths in fiber-based coherent SC.

**Funding.** National Foundation for Science and Technology Development (103.03-2020.19).

**Disclosures.** The authors declare no conflicts of interest.

**Data Availability.** Data underlying the results presented in this paper are not publicly available at this time but may be obtained from the authors upon reasonable request.

#### REFERENCES

1. J. M. Dudley, G. Genty, and S. Coen, "Supercontinuum generation in photonic crystal fiber," *Rev. Mod. Phys.* **78**, 1135–1184 (2006).
2. H. Pires, M. Baudisch, D. Sanchez, M. Hemmer, and J. Biegert, "Ultrashort pulse generation in the mid-IR," *Prog. Quantum Electron.* **43**, 1–30 (2015).
3. S. V. Smirnov, J. D. Ania-Castanon, T. J. Ellingham, S. M. Kobtsev, S. Kukarin, and S. K. Turitsyn, "Optical spectral broadening and supercontinuum generation in telecom applications," *Opt. Fiber Technol.* **12**, 122–147 (2006).
4. J. M. Dudley and J. R. Taylor, *Supercontinuum Generation in Optical Fibers* (Cambridge University, 2010).
5. G. Agrawal, *Nonlinear Fiber Optics*, 5th ed. (Academic, 2012).
6. J. M. Dudley, "Coherence properties of supercontinuum spectra generated in photonic crystal and tapered optical fibers," *Opt. Lett.* **27**, 1180–1182 (2002).
7. A. M. Heidt, A. Hartung, G. W. Bosman, P. Krok, E. G. Rohwer, H. Schwoerer, and H. Bartelt, "Coherent octave spanning near-infrared and visible supercontinuum generation in all-normal dispersion photonic crystal fibers," *Opt. Express* **19**, 3775–3787 (2011).
8. A. Rampur, D.-M. Spangenberg, G. Stepniowski, D. Dobrakowski, K. Tarnowski, K. Stefańska, A. Paździor, P. Mergo, T. Martynkien, T. Feurer, M. Klimczak, and A. M. Heidt, "Temporal fine structure of all-normal dispersion fiber supercontinuum pulses caused by non-ideal pump pulse shapes," *Opt. Express* **28**, 16579–16593 (2020).
9. A. Medjouri, D. Abed, O. Ziane, and L. M. Simohamed, "Design and optimization of As<sub>2</sub>S<sub>5</sub> chalcogenide channel waveguide for coherent mid-infrared supercontinuum generation," *Optik* **154**, 811–820 (2018).

10. K. Saitoh, N. J. Florous, and M. Koshiba, "Theoretical realization of holey fiber with flat chromatic dispersion and large mode area: an intriguing defected approach," *Opt. Lett.* **31**, 26–28 (2006).
11. G. Stępniewski, J. Pniewski, D. Pysz, J. Cimek, R. Stepień, M. Klimczak, and R. Buczyński, "Development of dispersion-optimized photonic crystal fibers based on heavy metal oxide glasses for broadband infrared supercontinuum generation with fiber lasers," *Sensors* **18**, 4127 (2018).
12. K. Jiao, J. Yao, Z. Zhao, X. Wang, N. Si, X. Wang, P. Chen, Z. Xue, Y. Tian, B. Zhang, P. Zhang, S. Dai, Q. Nie, and R. Wang, "Mid-infrared flattened supercontinuum generation in all-normal dispersion tellurium chalcogenide fiber," *Opt. Express* **27**, 2036–2043 (2019).
13. H. Balani, G. Singh, M. Tiwari, V. Janyani, and A. K. Ghunawat, "Supercontinuum generation at 155  $\mu\text{m}$  in  $\text{As}_2\text{S}_3$  core photonic crystal fiber," *Appl. Opt.* **57**, 3524–3533 (2018).
14. K. Tarnowski, T. Martynkien, P. Mergo, K. Poturaj, G. Soboń, and W. Urbańczyk, "Coherent supercontinuum generation up to 22  $\mu\text{m}$  in an all-normal dispersion microstructured silica fiber," *Opt. Express* **24**, 30523–30536 (2016).
15. S. Kedenburg, A. Steinmann, R. Hegenbarth, T. Steinle, and H. Giessen, "Nonlinear refractive indices of nonlinear liquids: wavelength dependence and influence of retarded response," *Appl. Phys. B* **117**, 803–816 (2014).
16. H. Takahashi, I. Sugimoto, T. Takabayashi, and S. Yoshida, "Optical transmission loss of liquid-core silica fibers in the infrared region," *Opt. Commun.* **53**, 164–168 (1985).
17. R. Zhang, J. Teipel, and H. Giessen, "Theoretical design of a liquid-core photonic crystal fiber for supercontinuum generation," *Opt. Express* **14**, 6800–6812 (2006).
18. Z. Guo, J. Yuan, C. Yu, X. Sang, K. Wang, B. Yan, L. Li, S. Kang, and X. Kang, "Highly coherent supercontinuum generation in the normal dispersion liquid-core photonic crystal fiber," *Prog. Electromagn. Res. M.* **48**, 67–76 (2016).
19. V. C. Lanh, A. Anuszkiewicz, A. Ramaniuk, R. Kasztelanica, K. D. Xuan, V. C. Long, M. Trippenbach, and R. Buczyński, "Supercontinuum generation in photonic crystal fibres with core filled with toluene," *J. Opt.* **19**, 125604 (2017).
20. Q. H. Dinh, J. Pniewski, H. Le Van, A. Ramaniuk, V. C. Long, K. Borzycki, K. D. Xuan, M. Klimczak, and R. Buczyński, "Optimization of optical properties of photonic crystal fibers infiltrated with carbon tetrachloride for supercontinuum generation with subnanosecond femtosecond pulses," *Appl. Opt.* **57**, 3738–3746 (2018).
21. V. T. Hoang, R. Kasztelanica, A. Filipkowski, G. Stępniewski, D. Pysz, M. Klimczak, S. Ertman, V. C. Long, T. R. Woliński, M. Trippenbach, K. D. Xuan, M. Śmietana, and R. Buczyński, "Supercontinuum generation in an all-normal dispersion large core photonic crystal fiber infiltrated with carbon tetrachloride," *Opt. Mater. Express* **9**, 2264–2278 (2019).
22. C. Van Lanh, V. T. Hoang, V. C. Long, K. Borzycki, K. D. Xuan, V. T. Quoc, M. Trippenbach, R. Buczyński, and J. Pniewski, "Optimization of optical properties of photonic crystal fibers infiltrated with chloroform for supercontinuum generation," *Laser Phys.* **29**, 075107 (2019).
23. L. C. Van, V. T. Hoang, V. C. Long, K. Borzycki, K. D. Xuan, V. T. Quoc, M. Trippenbach, R. Buczyński, and J. Pniewski, "Supercontinuum generation in photonic crystal fibers infiltrated with nitrobenzene," *Laser Phys.* **30**, 035105 (2020).
24. M. Chemnitz, C. Gaida, M. Gebhardt, F. Stutzki, J. Kobelke, A. Tünnermann, J. Limpert, and M. A. Schmidt, "Carbon chloride-core fibers for soliton mediated supercontinuum generation," *Opt. Express* **26**, 3221–3235 (2018).
25. H. Van Le, V. T. Hoang, H. T. Nguyen, V. C. Long, R. Buczyński, and R. Kasztelanica, "Supercontinuum generation in photonic crystal fibers infiltrated with tetrachloroethylene," *Opt. Quantum Electron.* **53**, 1–18 (2021).
26. H. Le Van, R. Buczyński, V. C. Long, M. Trippenbach, K. Borzycki, A. N. Manh, and R. Kasztelanica, "Measurement of temperature and concentration influence on the dispersion of fused silica glass photonic crystal fiber infiltrated with water–ethanol mixture," *Opt. Commun.* **407**, 417–422 (2018).
27. B. Guo, Y. Wang, C. Peng, H. L. Zhang, G. P. Luo, H. Q. Le, C. Gmachl, D. L. Sivco, M. L. Peabody, and A. Y. Cho, "Laser-based mid-infrared reflectance imaging of biological tissues," *Opt. Express* **12**, 208–219 (2004).
28. Y. T. Kuo, P. Y. Huang, Y. C. Li, J. L. Tang, and T. H. Wei, "Picosecond nonlinear refraction of  $\text{C}_2\text{H}_4\text{Cl}$  and  $\text{C}_2\text{H}_4\text{Br}_2$  at 532 nm studied with Z-scan technique," *J. Nonlinear Opt. Phys. Mater.* **27**, 1850015 (2018).
29. D. Milam, "Review and assessment of measured values of the nonlinear refractive-index coefficient of fused silica," *Appl. Opt.* **37**, 546–550 (1998).
30. Lumerical Solutions, Inc., <http://www.lumerical.com/tcad-products/mode/>.
31. S. R. Kachiraju and D. A. Gregory, "Determining the refractive index of liquids using a modified Michelson interferometer," *Opt. Laser Technol.* **44**, 2361–2365 (2012).
32. C. J. Knill and J. F. Kennedy, "CRC handbook of data on organic compounds," *Carbohydr. Polym.* **26**, 243–244 (1995).
33. L. Schneebeli, K. Kieu, E. Merzlyak, J. M. Hales, A. DeSimone, J. W. Perry, R. A. Norwood, and N. Peyghambarian, "Measurement of the Raman gain coefficient via inverse Raman scattering," *J. Opt. Soc. Am. B.* **30**, 2930–2939 (2013).
34. T. Shinoda, "Observations during the process of transition and melting for 1,2-dibromoethane by means of Raman spectroscopy," *Mol. Cryst. Liq. Cryst.* **35**, 191–203 (1976).
35. P. Zhao, M. Reichert, S. Benis, D. J. Hagan, and E. W. Van Stryland, "Temporal and polarization dependence of the nonlinear optical response of solvents," *Optica* **5**, 583–594 (2018).
36. B. Sierro and A. M. Heidt, "Noise amplification in all-normal dispersion fiber supercontinuum generation and its impact on ultrafast photonics applications," *OSA Contin.* **3**, 2347–2361 (2020).
37. I. B. Gonzalo, R. D. Engelholm, M. P. Sørensen, and O. Bang, "Polarization noise places severe constraints on coherence of all-normal dispersion femtosecond supercontinuum generation," *Sci. Rep.* **8**, 6579 (2018).
38. E. Genier, P. Bowen, T. Sylvestre, J. M. Dudley, P. M. Moselund, and O. Bang, "Amplitude noise and coherence degradation of femtosecond supercontinuum generation in all-normal-dispersion fibers," *J. Opt. Soc. Am. B.* **36**, A161–A167 (2019).
39. I. Bravo Gonzalo and O. Bang, "Role of the Raman gain in the noise dynamics of all-normal dispersion silica fiber supercontinuum generation," *J. Opt. Soc. Am. B.* **35**, 2102–2110 (2018).
40. N. Singh, M. Xin, D. Vermeulen, K. Shtyrkova, N. Li, P. T. Callahan, E. S. Magden, A. Ruocco, N. Fahrenkopf, C. Baiocco, B. P. P. Kuo, S. Radic, E. Ippen, F. X. Kärtner, and M. R. Watts, "Octave-spanning coherent supercontinuum generation in silicon on insulator from 1.06  $\mu\text{m}$  to beyond 2.4  $\mu\text{m}$ ," *Light Sci. Appl.* **7**, 17131 (2018).